

Article

Terahertz Replica Generation of Ultra-High Data Rate Transmission in an Electro-Optical Semiconductor Optical Amplifier Mach–Zehnder Interferometer System

Hassan Termos ^{1,2,*}  and Ali Mansour ² 

¹ ICFO—The Institute of Photonic Sciences, 08860 Barcelona, Spain

² ENSTA Bretagne, 2 Rue François Verny, CEDEX 09, 29806 Brest, France; ali.mansour@ensta-bretagne.fr

* Correspondence: hassan.termos@ensta-bretagne.fr

Abstract: This article presents an analysis of an electro-optical up-converter relying on a semiconductor optical amplifier Mach–Zehnder interferometer (SOA-MZI). The pulsed control signal is generated by an optical pulse clock (OPC) with a repetition rate of $f_s = 19.5$ GHz. The intermediate frequency (IF) signal, which carries the modulation format known as quadratic phase shift keying (QPSK) at a frequency f_{IF} , is shifted at the output of the SOA-MZI to high outlet mixing frequencies $nf_s \pm f_{IF}$, where n represents the harmonic order of the OPC. To examine the characteristics of the sampled QPSK signals, we employ the Virtual Photonics Inc. (VPI) emulator and evaluate them using significant metrics like error vector magnitudes (EVMS), conversion gains, and bit error rates (BERs). The up-mixing process is mainly achieved through the cross-phase modulation (XPM) effect in the SOA-MZI, which operates within a 195.5 GHz ultrahigh frequency (UHF). The electro-optical SOA-MZI up-converter demonstrates consistent uplifting conversion gains across the scope of the output mixing frequencies. The simulated conversion gain deteriorates from 38 dB at 20 GHz to 13 dB at 195.5 GHz. The operational efficiency of the electro-optical SOA-MZI design, employing the standard modulation approach, is also evaluated by measuring the EVM values. The EVM attains a 24% performance level at a data rate of 5 Gbit/s in conjunction with the UHF of 195.5 GHz. To corroborate our results, we compare them with real-world experiments conducted with the UHF of 59 GHz. The maximum frequency range of 1 THz is attained by increasing the OPC repetition rate. Ultimately, through elevating the control frequency to 100 GHz, the generation of terahertz replicas of the 4096-QAM (quadrature amplitude modulation) compound signal becomes achievable at heightened UHF, extending 1 THz, while maintaining a data transmission rate of 120 Gbit/s and upholding exceptional performance characteristics.

Keywords: electro-optical up-mixing; standard modulation topology; semiconductor optical amplifier Mach–Zehnder interferometer; quadrature amplitude modulation



Citation: Termos, H.; Mansour, A. Terahertz Replica Generation of Ultra-High Data Rate Transmission in an Electro-Optical Semiconductor Optical Amplifier Mach–Zehnder Interferometer System. *Photonics* **2024**, *11*, 83. <https://doi.org/10.3390/photonics11010083>

Received: 24 November 2023

Revised: 8 January 2024

Accepted: 12 January 2024

Published: 17 January 2024



Copyright: © 2024 by the authors. Licensee MDPI, Basel, Switzerland. This article is an open access article distributed under the terms and conditions of the Creative Commons Attribution (CC BY) license (<https://creativecommons.org/licenses/by/4.0/>).

1. Introduction

Terahertz (THz) and millimeter-wave (MMW) regions of the electromagnetic spectrum find applications in various fields. The MMW carrier technologies have experienced significant growth due to their recognized capacity for high-speed data transmission [1,2]. Furthermore, several effective mixing devices may generate high-power radio frequency (RF) pulses at ultrahigh frequency (UHF) approaching 1.5 THz [3–5]. On the contrary, radio over fiber (RoF) technologies have garnered considerable interest in RF signal transmission, offering advantages such as low loss distribution, compact size, and a wide spectrum. This technology can be utilized in various fields, including wireless fidelity (WiFi), surveillance radar systems [6], cellular networks, and satellite connections.

In the realm of RF connectivity, RoF, and MMW structures, the function of mixing is crucial for shifting the intermediate-frequency (IF) data spectrum to higher frequency ranges.

To achieve this, various types of mixers can be employed, including electrical, optical, or electro-optical mixers. Numerous methods can be used for photonic signal up-conversion, utilizing mixing processors, including an electro-optic modulator (EOM) [7,8], an electro-absorption modulator (EAM) [9] that can be used as an up-converter [10], and a photodiode (PD) [11,12]. Moreover, a range of all-optical frequency transformation techniques [13–16] capitalizes on the nonlinear attributes of an efficient semiconductor optical amplifier (SOA). For the employment of a SOA-MZI (SOA-Mach–Zehnder interferometer), the nonlinear cross-phase modulation (XPM) mechanism is employed for the up-conversion [17,18], and to complete the duplex purposes, both up- and down-conversions can be achieved [19]. Photonic transmission technologies also offer options for frequency mixing through sampling techniques [20–23]. SOA-MZIs can also be used for the gate functions [24,25] in the ripple carry adder design [26].

All-optical mixing is achieved in these various concepts due to the nonlinear characteristics of the mixers. To achieve mixing, another approach consists of manipulating the SOA electrical port. Two scenarios are applied: the standard modulation scenario, involving only one branch of the SOA-MZI; or the differential modulation scenario, involving both branches of the employed SOA-MZI. In the photonic standard SOA-MZI modulation, the carrier density of the top SOA is modified, whereas in the photonic differential SOA-MZI modulation, the carrier densities of the upper and lower SOAs are altered. As a result, changes in carrier density also modulate the photonic gain. The sampling and the IF or RF signals, requiring up- or down-conversion, can both be processed simultaneously on the same device [27,28].

In real-world experiments and simulations, we are exploring innovative electro-optical up-converters within the standard modulation structure of a SOA-MZI, which is an extension to our previous work [28] based on photonic differential SOA-MZI modulation. The central receptacle of the administered SOA-MZI is designed to allow the ingress of the sampling signal into the active area of SOA1, while the IF electric subcarrier controls the electric terminal of SOA1. The proposed electro-optical sampled signal dependent on the photonic SOA-MZI exhibits characteristics such as a wide bandwidth and a high conversion efficiency. To further assess the effectiveness and the quality of this electro-optical switching system employing the requested standard modulation approach, we initially obtain simulation results, including error vector magnitudes (EVMs), conversion gains, and bit error rates (BERs), using the VPI emulator. To validate these simulations within the frequency scope up to 59 GHz, we set up experiments based on a photonic SOA-MZI apparatus sourced from the Center for Integrated Photonics (CIP) company.

The groundbreaking approach employed in this study has enabled us to analyze EVMs with a data transfer rate of 5 Gbit/s, achieve an impressive frequency scalability of approximately 195.5 GHz, and obtain conversion gains at the discharge location of the operationalized SOA-MZI. These are the key advantages of our current research. This novel method opens up a range of potential applications, including wireless access [29], MMW and microwave connectivity, and ultra-wideband communication. Implementing the standard modulation approach provides significant benefits, such as expansive bandwidth, superior conversion efficiency, and minimal inlet energy prerequisites.

2. Electro-Optical Basic Concept of Architectural Standard Modulation

The design of the SOA-MZI utilized in our experimental observations and simulations is depicted in Figure 1. The simulated outcomes are achieved using a VPI emulator. A SOA-MZI mixing investigation based on the VPI application was originally introduced in our earlier research [30,31]. In each arm of the MZI, there is a semiconductor optical amplifier (SOA). Both output arms benefit from phase stabilization achieved by incorporating a phase-shifting element situated in each arm's top section. To the best of our knowledge, Figure 1 is the first depiction of the operational principle of the SOA-MZI standard modulation design for electro-optical mixing. In previous work, we utilized the sampling technique to explain the up-conversion process; you can find more details in [20]. Additionally, our

previous setup [28] elaborates on the methodology used in the electro-optical up-converter constructed with SOA-MZI employing differential modulation.

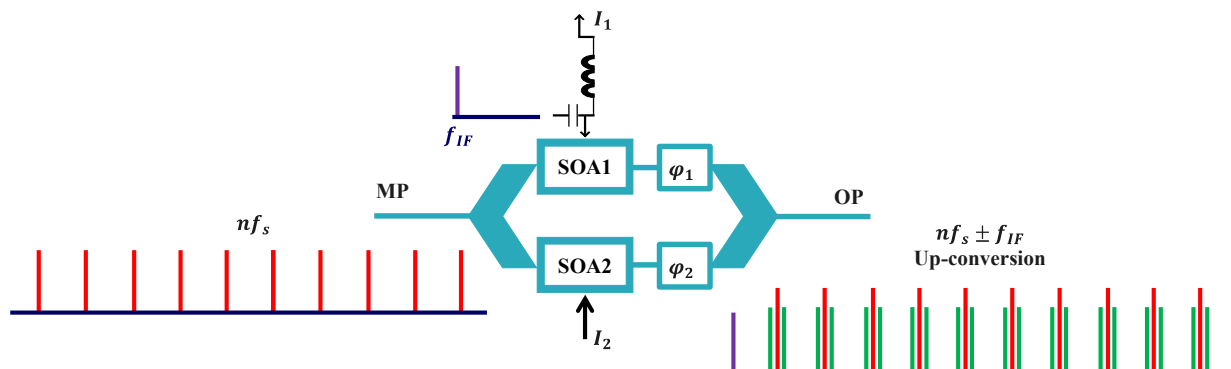


Figure 1. High-frequency electro-optical mixing relying on a photonic SOA-MZI apparatus using a conventional modulation method. MP: Middle Port; OP: Output Port; SOA: Semiconductor Optical Amplifier; and IF: Intermediate Frequency. n : represents the harmonic order of the control pulsed signal. The harmonics of the OPC are depicted in red, while the replicas of the sampled signal are represented in green.

In the standard modulation approach, the sampling signal, transmitted by an optical pulse clock (OPC) at a specific sampling frequency f_s and a wavelength λ_s , undergoes splitting at the median port (MP) of the SOA-MZI into two identical copies. Furthermore, the spectral elements of the sampling captured signal experience upward conversion in conjunction with the intermediate-stage signal. Importantly, there is no constraint on the repetition rate being within the modulation bandwidth of the SOA-MZI, allowing operation at frequencies that are abundant, as required for MMW applications [32]. In recent work, we used a data acquisition rate of $f_s = 19.5$ GHz [23]. Consequently, as the sampling interval rises, the photonic transmission efficiency is significantly improved [33].

The intermediate frequency (IF) photon is applied to the SOA electrode, where it modulates the steady-state current (bias current) with a specific intermediate frequency, denoted as f_{IF} , as shown in Figure 1. Quadrature Phase Shift Keying (QPSK) data can be transmitted over this electric subcarrier. This variation in the steady-state current leads to changes in the carrier density, allowing the IF signal to control the sampling signal immediately [20]. Since the optical gain of SOA1 is contingent on the carrier density, the enhanced sampling signal is continuously varied. This variation can be observed at the top and bottom ports, indicating that it is modified using the data channel. Consequently, the sampled signal exiting SOA1 and the amplified sampling captured signal from SOA2 are integrated at the terminal of the SOA-MZI. This is achieved following photonic filtering at the wavelength λ_s to generate the up-shifted photon. The resultant sampled photon contains frequency components of the sampling signal and is present at mixing frequencies $nf_s \pm f_{IF}$, where n varies from 1 to 10.

Electro-optical mixing, particularly when implemented using a SOA-MZI standard modulation, offers several compelling benefits compared to its all-optical counterpart [20,23]. One significant advantage lies in its inherent compatibility with established electronic signal processing techniques, allowing seamless integration into existing electronic systems. The ability to convert optical signals to electrical ones facilitates the precise control and manipulation of the signals, enabling advanced modulation and signal shaping. This feature proves advantageous in applications where intricate signal processing, format conversion, or regeneration are essential. Additionally, electro-optical mixing provides a versatile platform, accommodating a wide range of modulation formats and enabling the exploitation of electronic technologies for real-time adaptive control. The incorporation of electronic components, though introducing some complexity, often results in improved signal quality and reliability. Overall, the benefits of electro-optical mixing, especially in terms of compat-

ibility, control, and adaptability, make it a preferred choice for applications requiring the synergy of optical and electronic signal processing within a SOA-MZI framework.

3. Operational Efficiency of the Electro-Optical Up-Shifting Arrangement Utilizing a Classical Modulation Topology with a SOA-MZI

A. Electro-Optical Mixing Setup

Figure 2 depicts the arrangement for the electro-optical upward conversion. In our investigation, the electrical interface of SOA1 introduces the intermediate frequency (IF) signal (data signal). The steady-state current and the modulated data photon are combined to control the SOA electrode. The bias current across both SOAs is set to 400 mA. Furthermore, the electrical interface of SOA1 is configured with 50Ω impedance. The laser source (LS) produces the data signal with specific parameters, such as a wavelength of 1545 nm and an average optical power of -15 dBm. The Mach-Zehnder modulator (MZM) transforms the optical light (data signal) using the M-QAM (quadrature amplitude modulation) data format, supplied by an electrical subcarrier (auxiliary carrier) at its electrical interface at $f_{IF} = 0.5$ GHz. The electrical power of the incoming data modulation is set to 13 dBm at the MZM electrical port. For the experimental work, the IF signal can be generated using an arbitrary waveform generator (AWG) as indicated (1) in Figure 2, or for simulations, a Generation and Detection Module mentioned (2) in Figure 2 at the MZM electrical gate. Subsequently, the optical M-QAM modulated signal at the MZM output undergoes conversion to the electrical domain using the first photodiode (PD1) with a sensitivity of 0.85 A/W. This electrical signal is then subject to amplification through a 33 dB gain from the first low-noise amplifier (LNA1) before being introduced into the electrical port of the upper SOA (SOA1).

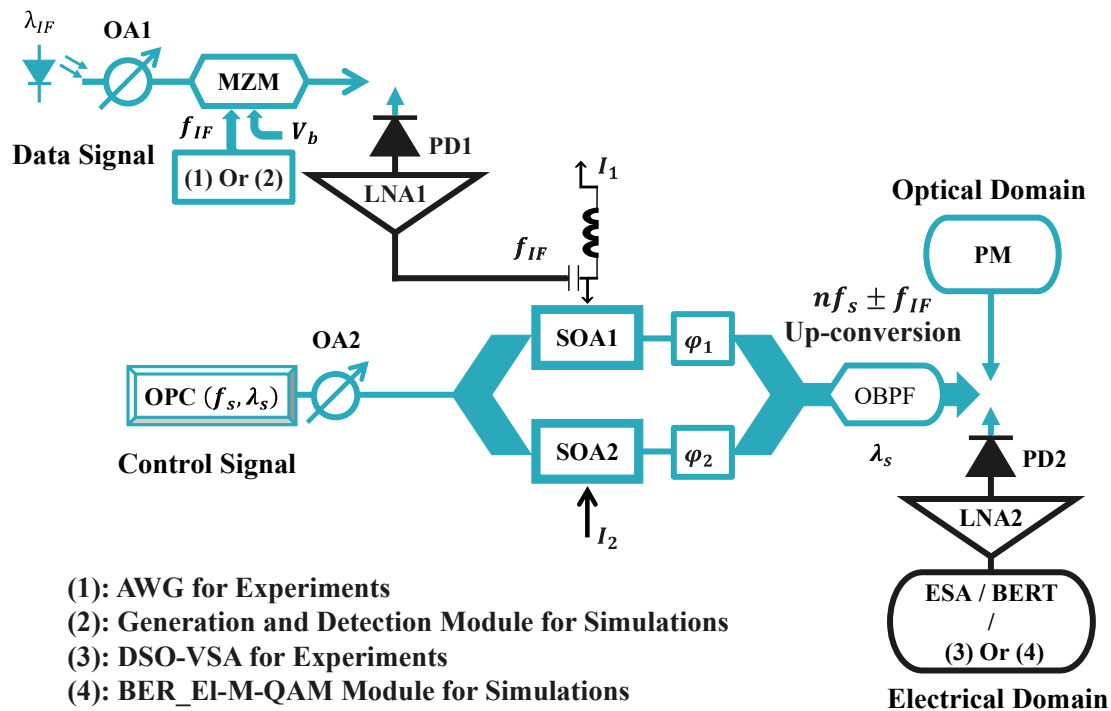


Figure 2. Frequency up-mixing setup dependent on the SOA-MZI standard modulation approach. The optical devices are depicted in a greenish-blue color, while the electrical devices are represented in black. AWG: Arbitrary Waveform Generator, BER: Bit Error Rate, BERT: Bit Error Rate Tester, DSO: Digital Sampling Oscilloscope, LNA: Low-Noise Amplifier, ESA: Electrical Spectrum Analyzer, MZM: Mach-Zehnder Modulator, OA: Optical Attenuator, OBPF: Optical Band Pass Filter, OPC: Optical Pulse Clock, PD: Photodiode, PM: Power Meter, QAM: Quadrature Amplitude Modulation, VSA: Vector signal Analyzer, and V_b : Bias Voltage.

The employed AWG, sourced from Keysight Technologies, Inc. under the model M8194A [34], embodies an exceptional fusion of celerity, bandwidth, and channel density within a singular module. Meticulously crafted to fulfill the distinct requirements of M-QAM modulation formats, it excels, with sample rates reaching up to 120 gigasamples per second (GSa/s). Recognized as one of Keysight's high-velocity AWGs, the M8194A achieves a harmonious equilibrium between versatility and simplicity, ensuring seamless operation in both solitary and multi-channel configurations. Orchestrated by a personal computer (PC) via a universal serial bus (USB), the AWG module introduces the preferred M-QAM format at an IF or RF frequency using a specific code that delineates the number of states in the QAM data and the IF/RF frequency. In our exploration, we generate four QPSK as well as 4096-QAM formats at varying baud rates or symbol rates (SRs) of up to 10 gigabauds (GBd) or (GSymb/s). Noteworthy is the AWG's prowess in generating M-QAM data at heightened baud rates, extending impressively up to 100 (GBd).

An optical pulse clock (OPC) with a wavelength of $\lambda_s = 1550$ nm generates the required sampling signal at a repetition rate of $f_s = 19.5$ GHz at a pulse width of 1.6 ps. This signal is connected to the SOA-MZI's Medium Port (MP) interface. This repetition frequency is also changed to $f_s = 100$ GHz in order to achieve terahertz up-mixing. Harmonics are shown in the electrical spectrum at $H_n = nf_s$. By utilizing an optical attenuator (OAtt), electro-optical mixing is achieved by reducing the peak sampling power to -1 dBm. Based on the information provided, it appears that the optimal electrical spectrum is obtained at this power level.

The outlet of the SOA-MZI is equipped with an optical band-pass filter (OBPF) configured at 1550 nm, featuring a bandwidth of 0.6 nm. In the optical domain, the filtered up-converted signal is directly linked to a power meter (PM) to gauge its power output. In the electrical domain, the sampled signal is now detected by a 300 GHz second PD (PD2) with a sensitivity of 0.85 A/W. Following this, the signal gets strengthened by the second LNA (LNA2), which has an output gain of 33 dB. An electrical spectrum analyzer (ESA) is used to evaluate the accomplishments of the up-mixed transmission. During the simulations, the bit error rate (BER) evaluation for the electrically sampled M-ary QAM (BER_EL-M-QAM) section that is mentioned as (4) in Figure 2 is applied to determine the requested error vector magnitude (EVM) values using the VPI emulator [35]. The experiment uses a specialized tool called a digital sampling oscilloscope (DSO) and an application known as a vector signal analyzer (VSA), marked as (3) in Figure 2. This setup helps gather data on two important measures: EVMs and BERs. Moreover, one could incorporate an optical coupler (OC) at the OBPF's exit to examine the blending efficiency of the system simultaneously in both the optical and electrical realms. As an OC can divide the optical power into a 50/50 or 10/90 ratio, depending on the specific OC, there is also consideration for associated losses. Nonetheless, this practice is sidestepped to enhance not only the signal quality but also the overall performance of the system. It is noteworthy to mention that the utilized photodiodes (PD1 and PD2) are recognized as uni-traveling carrier (UTC) PDs (UTC-PDs), specifically chosen for their role in photodetection [36–38].

To compare the experiment results to the simulated ones, the authentic SOA-MZI from the Center for Integrated Photonics (CIP) is utilized, along with various additional components for experimental characterization. Furthermore, to perform a reliable comparison between the experimental and simulated investigations, all the operational points used in the simulations are replicated in the configuration. It is crucial to emphasize that the experimental arrangement is constrained by the bandwidth of the ESA. Consequently, the frequency scope is capped at a maximum of 59 GHz. For the purpose of comparing the up-converted transmissions between the experiments and simulated results, the resultant incorporating frequency values varying from $f_s + f_{IF} = 20$ GHz to $3f_s + f_{IF} = 59$ GHz are considered. The maximum achieved bandwidth is $10f_s + f_{IF} = 1.005$ THz when $f_s = 100$ GHz.

Incorporating the SOA-MZI standard modulation mode into photonic networks is a significant achievement, enabling effective electro-optical mixing, which is a critical compo-

ponent in essential wavelength-division multiplexing (WDM) technologies. Electro-optical mixing has far-reaching implications, particularly in the realm of signal analysis, where it enhances both data transmission speed and efficiency. SOA-MZI devices, utilizing interactions such as XPM and XGM, achieve ultrafast switching in the picosecond or femtosecond dimensions, leveraging the quick reaction times of SOAs (SOA1 and SOA2). These devices, integral components of photonic integrated circuits (PICs), play a crucial role in advancing optical technology systems, especially RoF and MMW applications. Furthermore, within the industry landscape, quantum information processing [39–44] presents an opportunity to explore and assess SOA-MZI systems, particularly in applications like quantum key distribution (QKD).

B. Optical Conversion Gain Features

The terminus of the photonic SOA-MZI defines the outbound photonic power for the up-mixed field, determined by the applied electro-optical standard modulation design, and quantified at 29.5 dBm through precise measurement with a power meter (PM). The optical conversion gain (OCG) of the up-lifted signal is determined by the difference between the outgoing mixed power of 29.5 dBm and the inlet data power of -15 dBm. In consequence, the electro-optical classical modulation technology can be assessed with an OCG number of 44.5 dB, which is efficiently considered a valuable outcome. It is important to highlight that the OCG holds a similar value in both the experimental and simulated investigations.

In our experimental or simulated arrangement, it is feasible to measure only a single output optical power value along with the optical input power using a PM. In such instances, a singular value for the OCG is obtained. Various approaches can be employed to assess the mixing system's performance for optimal results. Initially, the optical input power of the data signal is adjusted within the range of -30 to 15 dBm, establishing that the most favorable OCG outcome occurs at -15 dBm, as depicted in Figure 3 for the experimental and simulated results. Furthermore, adopting the standard modulation configuration with the OBPF set at 1550 nm, corresponding to the OPC wavelength, significantly enhances system quality, as evidenced in Figure 3.

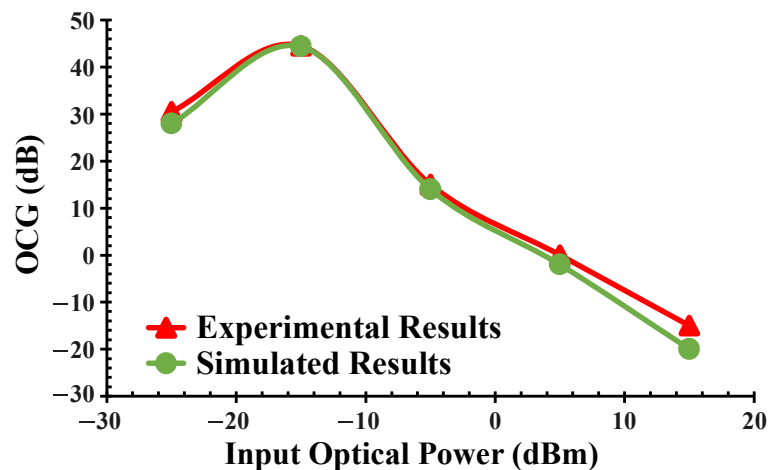


Figure 3. Experimental and simulated OPG as a function of the input optical power of the data signal.

Conversely, modifying the OBPF wavelength to 1545 nm, aligning with the data signal wavelength as shown in Figure 4, leads to a substantial 20 dB reduction in the OCG across the entire input power range for the experimental study. To address this issue, implementing the standard switching configuration, wherein the positions of the OPC and data signal are interchangeable, proves beneficial [30]. Consequently, the peak OCG of 44.5 dB is attained with an input optical power of -15 dBm for the data signal, aligning with the OBPF set at 1550 nm.

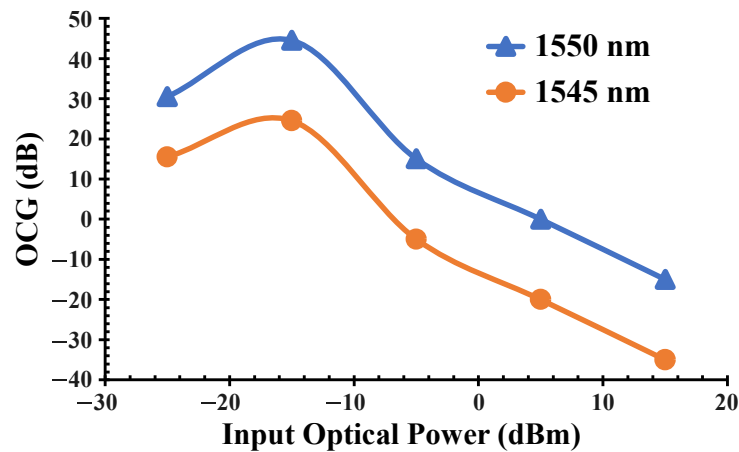


Figure 4. Experimental OPG as a function of the input optical power of the data signal when the OBPF is adjusted at two different wavelengths.

C. Electrical Conversion Gain Attributes

In both the simulated and experimental investigations, we display the electrical spectra of the up-converted signal at the outgoing of the SOA-MZI, as displayed in Figures 5 and 6, respectively. These results serve as evidence of the fundamental concept of the electro-optical standard modulation design. It is worth noting that the original input IF signals in both cases are up-converted at mixing frequencies $nf_s \pm f_{IF}$. In these scenarios, the amplitude of the multiple harmonics of the sampling captured signal gradually decreases with the harmonic rank. The simulation results depicted in Figure 5 show an approximately 8 dB distinction from the initial to the tenth harmonic due to the dynamic nature of the SOA-MZI [20,30,45]; this phenomenon cannot be avoided. Notably, the up-converted transmissions include the tenth harmonic of the sampling signal. Therefore, $10f_s + f_{IF} = 195.5$ GHz represents the highest frequency range achieved in Figure 5.

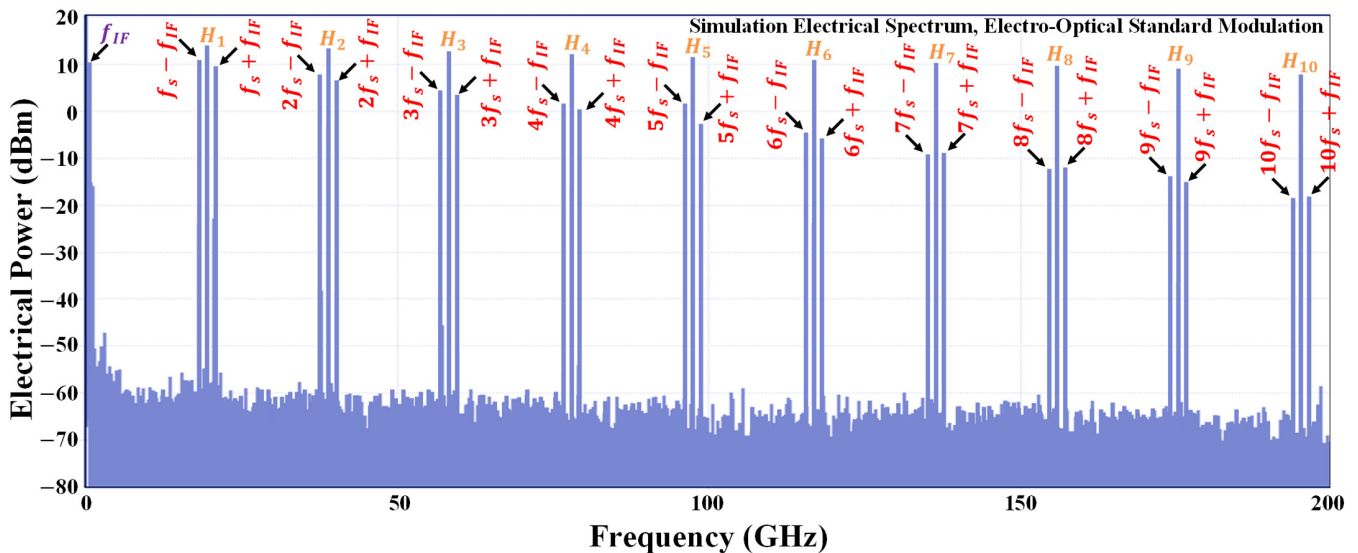


Figure 5. Electrical spectrum of the up-converted photon at mixing frequencies $nf_s \pm f_{IF}$ at the SOA-MZI outgoing for the applied standard modulation. The frequency of the IF signal is $f_{IF} = 0.5$ GHz, the sampling control frequency is $f_s = 19.5$ GHz, and the sampling signal harmonics at $H_n = nf_s$.

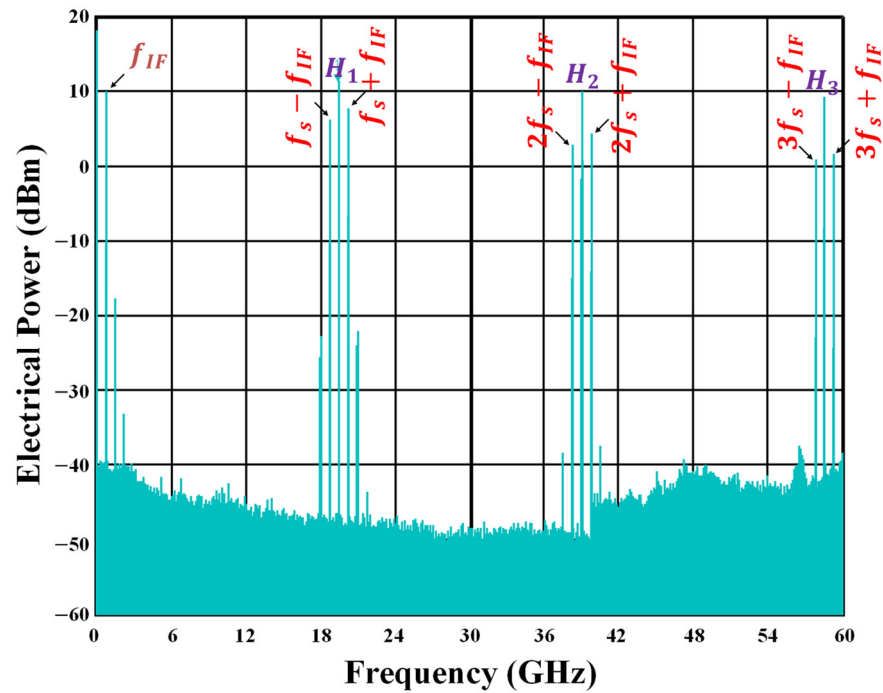


Figure 6. Experimental electrical spectrum achieved for the significant up-converted signal at $nf_s \pm f_{IF}$ at the SOA-MZI outlet for the standard modulation design, where n spans from 1 to 3.

The experimental exploration of the SOA-MZI standard modulation system is depicted in Figure 6, showcasing the representation of solely the initial three harmonics of the control signal alongside the replicas of the mixed signal. Consequently, the deterioration of the up-mixing replicas is fundamentally identical in both situations. In both cases, the up-converted signals track the control signal harmonics as they recede. The simulations shown in Figure 5 yield similar results. However, the simulation model exhibits more noticeable improvement in higher frequency ranges, extending up to 195.5 GHz.

The determination of the conversion efficiency involves assessing the difference in requested electrical powers between the up-lifted replicas at outgoing frequencies $nf_s + f_{IF}$ and the inlet signal measured at a frequency of $f_{IF} = 0.5$ GHz. This analysis provides an insight into the effectiveness of the up-mixed signal within the framework of designing electro-optical standard modulation systems.

Referring to Figure 7, the electrical conversion gain (ECG) undergoes a reduction in the simulation analysis from 38 dB at $f_s + f_{IF} = 20$ GHz to 13 dB at $10f_s + f_{IF} = 195.5$ GHz. This transition from the initial to the final ECG values shows a notable 25 dB difference. The ECGs of the up-converted signal in the experimental research presented in Figure 7 are limited to measurements at $f_s + f_{IF} = 20$ GHz, $2f_s + f_{IF} = 39.5$ GHz, and $3f_s + f_{IF} = 59$ GHz due to the constrained bandwidth of the used ESA. To confirm the results, a comparison is made with the corresponding range in simulated scenarios.

Because of the shot and thermal noise at the receiver, coupled with the optical fiber’s photonic inefficiencies, the ECG observed in real-world experiments is about 2 dB lower than the simulation ones. Our laboratory research corroborates the ECG findings in the actual environment when compared to the simulated data. Thanks to the SOA amplification gains and the involvement of mixing frequencies associated with the harmonics H_n , favorable ECG values are achieved over all mixing frequencies in both simulation and experimental measurements.

At substantial mixing frequencies, the ECG undergoes a notable decrease due to the dynamic conductance of the SOA-MZI [20]. Nevertheless, the amplification of electrical power at extreme mixing frequencies is influenced by the conventional modulation process and the increase in the OPC repetition rate, as presented in the following section [46].

Owing to the dynamic nature of the SOA-MZI, achieving parity between harmonic power and replica power becomes an important task.

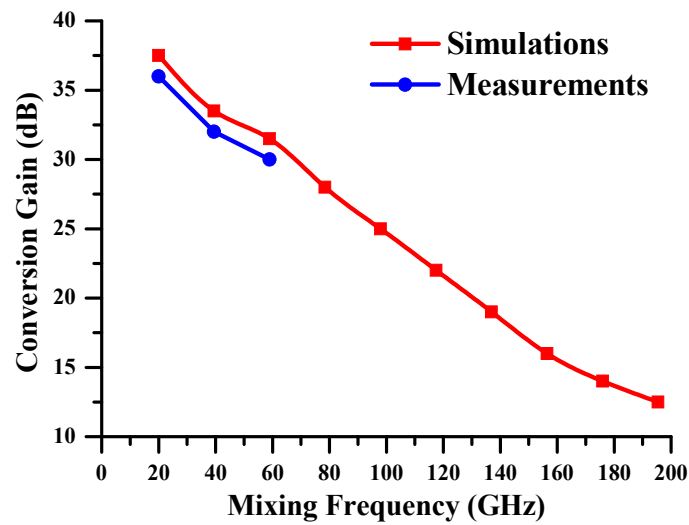


Figure 7. Electrical conversion gains at $nf_s + f_{IF}$ for experimental and simulation investigations contingent on the SOA-MZI standard modulation modes. The input IF signal at $f_{IF} = 0.5$ GHz is up-converted at $nf_s + f_{IF}$.

D. QPSK Frequency Up-Conversion Attributes

At a data transfer speed of 5 Gbit/s, we assess the efficacy of an electrical Quadrature Phase Shift Keying (QPSK) data subcarrier that has experienced frequency shifting to elevated frequencies. This evaluation is conducted through simulations at the outgoing portal of the SOA-MZI within the framework of the electro-optical standard modulation. The effectiveness of the applied mixing system is gauged by assessing the quality of the up-shifted signal through the error vector magnitude (EVM), offering valuable insights [47,48]. The bit error rate (BER) metric for the QPSK mixing transmission is conducted using the BER_EI-M-QAM arrangement integrated into the VPI software. These BER metrics appraise the excellence of the received signal, determining the EVM parameters for the recorded signal in the mixing process.

Following the application of error correction techniques (FEC), the established threshold for admissible BER is defined as 0.0038 [49]. Moreover, the EVM restriction for the QPSK data should not surpass 17.5% [50,51]. It is noteworthy that, for experimental purposes, the up-converted photon undergoes conversion into a digital format employing a contemporary digital sampling oscilloscope (DSO). Subsequently, the EVM of the recorded signal is evaluated utilizing vector signal analyzer (VSA) software. Additionally, the DSO-VSA instruments exhibit the capability to demodulate the up-mixed QPSK data at various mixing frequencies.

It is essential to emphasize that the optical outgoing power directly at the output portal of the SOA-MZI registers at 29.5 dBm. However, this power level undergoes a 3-dB reduction due to optical losses within the OBPF. At the SOA-MZI outlet, thermal and shot noises are generated during the conversion of the optical photon to the electrical one by the PD2. Subsequently, the electrical signal undergoes additional amplification using LNA2. Consequently, all computations for the EVM metric, as depicted in Figure 8, must account for the noise introduced during signal sampling, filtering, photodetection, and subsequent amplification.

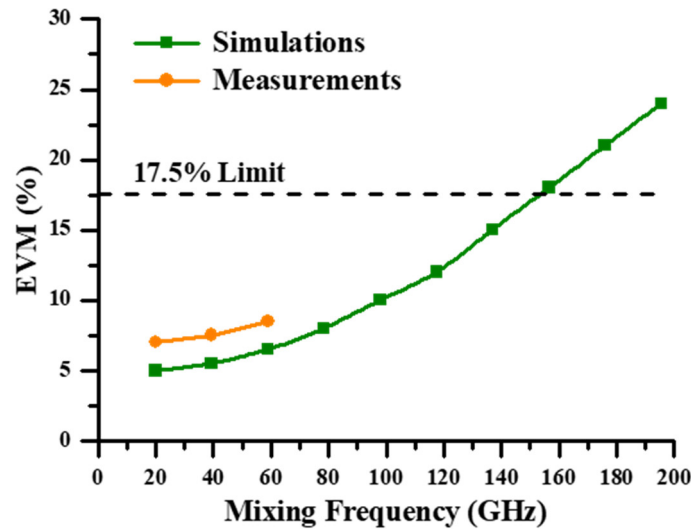


Figure 8. The EVM metric of QPSK shifted signals from $f_{IF} = 0.5$ GHz to $nf_s + f_{IF}$ at the data transfer rate of 5 Gbit/s for the empirical and simulated investigations.

Figure 8 illustrates that in both real-world and simulated measurements, the EVM of QPSK up-shifted signals varies with the mixing outgoing frequency at 5 Gbit/s. In simulations, it ranges from 5% at $f_s + f_{IF} = 20$ GHz to 24% at $10f_s + f_{IF} = 195.5$ GHz. In real-world measurements, due to unexpected noise, the EVMs are 2% higher than the simulated values over the limited range of mixing frequencies up to $3f_s + f_{IF} = 59$ GHz. However, with the exception of the highest mixing frequencies in simulations, all EVM values for the up-converted signals remain under the EVM criteria of 17.5%.

Within the electrical domain, the mixed signal, as illustrated in the electrical spectrums in Figures 5 and 6, exhibits multiple replicas. This enables the measurement of EVM and ECG for each frequency of these replicas. A higher ECG corresponds to improved EVM performance in our system, which also has an excellent OCG of 44.5 dB. On the other hand, the relationship between ECG and EVM is still nuanced because there is no direct link, and while a higher ECG indicates improved efficiency in the conversion process, the overall system performance, as assessed by EVM, depends on various factors, including signal quality and accuracy in the mixing and conversion process. Therefore, in the context of our system, a higher ECG may indeed correspond to improved efficiency in the conversion of replicas obtained by mixing through SOA-MZI, but it does not directly imply better EVM performance unless other factors influencing EVM are also considered. As a result, the ECG depends only on power, while the EVM depends on many other factors.

EVM in our communication system is influenced by a myriad of factors, each contributing to the accuracy and fidelity of the transmitted signal. Noise and distortion within the communication channel, nonlinearities in system components, and the presence of phase noise from signal sources are the primary contributors to increased EVM. Additionally, imperfections in modulation and demodulation processes, frequency and timing offsets, and variations in carrier frequency can introduce errors in both magnitude and phase. Signal impairments stemming from channel fading, dispersion, and multipath propagation, particularly in wireless or optical systems, further impact EVM. Consequently, a comprehensive assessment of EVM necessitates addressing these multifaceted influences through our meticulous system design, the incorporation of error correction techniques, and the optimization of components to minimize distortions and inaccuracies in the communication system. However, a lower output power leads to a lower ECG and, consequently, a higher EVM value.

4. Comparison of Electro-Optical Mixer Performances

In the context of the approach called standard modulation, electro-optical mixing is conducted through both experimental and simulation setups, as depicted in the aforementioned results. In both setups, an additional IF signal is introduced at the electrical terminal of SOA1. This configuration was originally established as part of the innovative differential modulation [28]. A comparative analysis between these methods is presented in Table 1, which substantiates that the differential modulation exhibits superior efficiency and quality, as evidenced by enhanced conversion gains and reduced EVMs, respectively.

Table 1. Comparison of SOA-MZI electro-optical mixer performances using standard and differential modulation approaches.

	Standard Modulation		Differential Modulation [28]	
	Simulation	Reality	Simulation	Reality
Frequency Limit (GHz)	195.5	59	195.5	59
Conversion Gain (dB)	13	30	25	34
EVM (%)	24	8.5	14	5.5
Data Rate (Gbit/s)	5	5	5	5

While acknowledging the groundbreaking achievement of implementing the standard modulation approach in the electro-optical SOA-MZI design for the first time, it is essential to highlight the major advantages it offers in comparison to the previously explored differential modulation method [20,23,28,33]. Firstly, standard modulation techniques are renowned for their simplicity and ease of implementation, making them particularly advantageous in scenarios where a straightforward system design is paramount. Furthermore, standard modulation schemes often demonstrate greater robustness against phase shifts, a critical factor for ensuring reliable communication. In the context of our all-optical and electro-optical systems, the differential approach may enhance the signal quality, thereby contributing to an overall improvement in data transmission performance. However, it is noteworthy that the stability achieved in the mixing operation is higher for the standard modulation, providing additional time for precise system performance measurements. Additionally, the widespread adoption of standard modulation techniques in the industry enhances the compatibility with existing systems and equipment. Despite the seemingly superior performance of the differential modulation approach in Table 1, the selection between standard and differential modulation hinges on specific system requirements, channel characteristics, and the desired equilibrium between complexity and performance.

5. Performance of Terahertz Replicas Generation

While increasing the OPC repetition rate can offer benefits in terms of higher data throughput as well as higher frequency range with excellent signal quality, it also presents challenges related to power consumption, synchronization, and cost in terms of components and the necessary infrastructure by building or upgrading the requested electro-optical mixing system. In our setup, we just change the OPC repetition rate to $f_s = 100$ GHz. This leads to the accomplishment of terahertz replica generation at mixing frequencies of up to $10f_s + f_{IF} \approx 1$ THz at the SOA-MZI output in both empirical and virtual investigations. The implementation of the experimental repetition rate principle has outstanding performance in terms of increasing the power and mitigating the noise [46]. To assess how well the system performs when operating at 1 THz, we measure the bit BER indicator [51] of the up-mixed field loading for two types of data modulations, which are QPSK and 4096-quadrature amplitude modulation (QAM), as a function of the symbol rate; see Figure 9. To measure the BER, we employ a dedicated device known as a bit error rate tester (BERT).

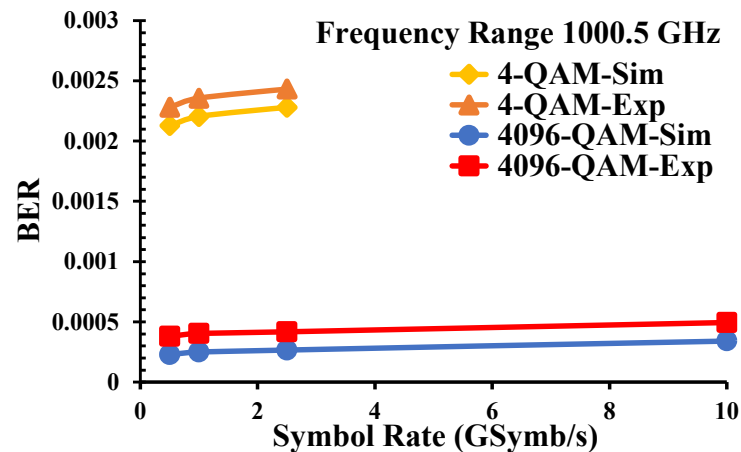


Figure 9. Experimental and simulated BER versus SR for 4- and 4096-QAM mixed signal. Sim: Simulation and Exp: Experimentation.

Figure 9 displays the BER performance in opposition to symbol rates of the achievable up-mixed signal. The highest recorded BER is 0.0024, corresponding to a 32% EVM for the QPSK signal at the baud rate or symbol rate (SR) of 2.5 GSymb/s in the experimental work, while it is 0.0023 at 2.5 GSymb/s for the imitated study. In contrast, it registers at 0.00034 for the 4096-QAM signal, equating to a 4.5% EVM at 10 GSymb/s in the simulation study, while it is 0.0005 at 10 GSymb/s in the experimental work. It is noteworthy that we observe an increase in BER as the SR rises for both systems. The actual BER is very similar to the simulated one, affirming the robust performance of the terahertz replica generation systems. Additionally, the distinctive characteristics of the employed SOAs and their physical components, including bias current, also impact the quality of the modulated light, as reflected in the BER values. The maximum bit transmission rate is 5 and 120 Gbit/s by loading 4- and 4096-QAM data for up mixing operations, respectively.

The electro-optical SOA-MZI system in our study faces several limitations that warrant further exploration in our future designs. One notable constraint lies in the nonlinear effects within SOAs, including gain saturation and XPM, in addition to the ASE noise, which can compromise signal quality and overall system performance. Additionally, the inherent bandwidth limitations of SOAs, particularly in the THz frequency range, pose challenges to achieving ultra-high data rates. The sensitivity of the system to temperature fluctuations, complexities in the alignment of the MZI, and potential integration issues with existing optical networks further contribute to the system’s limitations. Addressing these challenges in future research could involve strategies to mitigate nonlinearities, broaden the bandwidth of SOAs, enhance temperature stability, simplify MZI alignment, and improve overall system integration, thereby advancing the feasibility and efficiency of THz communication systems based on the electro-optical SOA-MZI architecture.

To achieve efficient mixing in a SOA-MZI system, a balance of both high and low nonlinearities is often sought. The SOA-MZI introduces nonlinearity due to effects such as gain saturation and XPM. These nonlinear effects play a crucial role in processes like signal amplification and frequency mixing. High nonlinearities in SOAs are desirable for effective mixing, as they contribute to the generation of harmonics and facilitate the nonlinear phase shift required for signal manipulation. However, an excessively high level of nonlinearity may lead to signal distortion and other undesirable effects. On the other hand, having some degree of low nonlinearity is also important to maintain the integrity of the signals and prevent excessive distortion. Achieving the right balance involves optimizing the SOA parameters, such as bias current and input power levels, to harness the benefits of nonlinear effects for mixing while mitigating their negative impact on signal quality. Therefore, future work in SOA-MZI systems should explore methods to fine-tune and control the nonlinearity to achieve efficient mixing without compromising overall system performance.

To address existing constraints, future investigations could focus on optimizing the system's efficiency and performance through novel design approaches, exploring advanced materials, and implementing optimization techniques for the SOA-MZI architecture. Additionally, there is room to enhance data rate capabilities and extend transmission distances by employing advanced modulation techniques, signal processing methods, and innovative compensation techniques to mitigate signal attenuation and dispersion challenges. Integration with emerging technologies, such as machine learning and quantum communication, could be explored for improved adaptability and security. Furthermore, research could delve into practical applications in fields like telecommunications, medical imaging, and industrial sensing, ensuring the technology's viability in real-world scenarios. In the end, considerations for standardization, interoperability, and addressing security vulnerabilities are essential components for comprehensive future research directions in THz communication systems.

Finally, a promising upcoming solution involves utilizing the OPC control signal within the attosecond domain, as opposed to the current 1.6 ps pulse width duration with an exceptionally high repetition rate. This solution may be used with the intention to overcome the dynamic behavior limitations associated with the use of SOA-MZI structures and enhance the overall mixing quality performance.

6. Conclusions

This investigation introduces an electro-optical fusion system employing the standard modulation dependent on the SOA-MZI at an exceptionally high frequency range, extending up to 195.5 GHz. The architecture efficiency is evaluated based on optical and electrical conversion gains. With QPSK data, the system exhibits achievable EVMs for very high bit transmission rates, up to 5 Gbit/s. Specifically, when the mixed QPSK field is generated at 5 Gbit/s, the EVM reaches 24% at 195.5 GHz. A comparative analysis between the simulated findings and real-world experiments reveals similar outcomes. Moreover, by increasing the control frequency to 100 GHz, it becomes possible to generate terahertz 4096-QAM up-mixing replicas up to 1 THz, with 120 Gbit/s, while maintaining excellent performance characteristics.

Author Contributions: H.T. performed the principle, experiments, and simulations and prepared the manuscript; A.M. reviewed the manuscript. All authors have read and agreed to the published version of the manuscript.

Funding: This research received no external funding.

Institutional Review Board Statement: Not applicable.

Informed Consent Statement: Not applicable.

Data Availability Statement: Data underlying the results presented in this paper are not publicly available at this time but may be obtained from the authors upon reasonable request.

Conflicts of Interest: The authors declare no conflicts of interest.

References

1. Kleine-Ostmann, T.; Nagatsuma, T. A review on terahertz communications research. *J. Infrared Millim. Terahertz Waves* **2011**, *32*, 143–171. [[CrossRef](#)]
2. Stöhr, A.; Babel, S.; Cannard, P.J.; Charbonnier, B.; van Dijk, F.; Fedderwitz, S.; Moodie, D.; Pavlovic, L.; Ponnampalam, L.; Renaud, C.C.; et al. Millimeter-wave photonic components for broadband wireless systems. *IEEE Trans. Microw. Theory Tech.* **2010**, *58*, 3071–3082. [[CrossRef](#)]
3. Rouvalis, E.; Renaud, C.C.; Moodie, D.G.; Robertson, M.J.; Seeds, A.J. Travelling-wave uni-travelling carrier photodiodes for continuous wave THz generation. *Opt. Express* **2010**, *18*, 11105–11110. [[CrossRef](#)] [[PubMed](#)]
4. Ito, H.; Kodama, S.; Muramoto, Y.; Furuta, T.; Nagatsuma, T.; Ishibashi, T. High-speed and high-output InP-InGaAs unitraveling-carrier photodiodes. *IEEE J. Sel. Top. Quantum* **2004**, *10*, 709–727. [[CrossRef](#)]
5. Preu, S.; Döhler, G.H.; Malzer, S.; Wang, L.J.; Gossard, A.C. Tunable, continuous-wave terahertz photomixer sources and applications. *J. Appl. Phys.* **2011**, *109*, 061301. [[CrossRef](#)]

6. Thomas, V.A.; El-Hajjar, M.; Hanzo, L. Millimeter-wave radio over fiber optical upconversion techniques relying on link nonlinearity. *IEEE Commun. Surv. Tutor.* **2016**, *18*, 29–53. [[CrossRef](#)]
7. Sun, C.K.; Orazi, R.J.; Pappert, S.A.; Burns, W.K. A photonic-link millimeter-wave mixer using cascaded optical modulators and harmonic carrier generation. *IEEE Photonics Technol. Lett.* **1996**, *8*, 1166–1168. [[CrossRef](#)]
8. Schaffer, C.G.; Sauer, M.; Kojucharow, K.; Kaluzni, H. Increasing the channel number in WDM mm-wave systems by spectral overlap. In Proceedings of the International Topical Meeting on Microwave Photonics MWP 2000 (Cat. No.00EX430), Oxford, UK, 11–13 September 2000; pp. 164–167.
9. Kuri, T.; Kitayama, K.; Ogawa, Y. Fiber-optic millimeter-wave uplink system incorporating remotely fed 60-GHz band optical pilot tone. *IEEE Trans. Microw. Theory Tech.* **1999**, *47*, 1332–1337. [[CrossRef](#)]
10. Park, C.S.; Oh, C.K.; Lee, C.G.; Kim, D.-H.; Park, C.-S. A photonic up-converter for a WDM radio-over-fiber system using cross-absorption modulation in an EAM. *IEEE Photonics Technol. Lett.* **2005**, *17*, 1950–1952. [[CrossRef](#)]
11. Tsuchiya, M.; Hoshida, T. Nonlinear photodetection scheme and its system applications to fiber-optic millimeter-wave wireless down-links. *IEEE Trans. Microw. Theory Tech.* **1999**, *47*, 1342–1350. [[CrossRef](#)]
12. Paresys, F.; Shao, T.; Maury, G.; Le Guennec, Y.; Cabon, B. Bidirectional millimeter-wave radio-over-fiber system based on photodiode mixing and optical heterodyning. *IEEE/OSA J. Opt. Commun. Netw.* **2013**, *5*, 74–80. [[CrossRef](#)]
13. Seo, Y.-K.; Choi, C.-S.; Choi, W.-Y. All-optical signal up-conversion for radio-on-fiber applications using cross-gain modulation in semiconductor optical amplifiers. *IEEE Photonics Technol. Lett.* **2002**, *14*, 1448–1450. [[CrossRef](#)]
14. Jung, H.; Chigo-Okonkwo; Tangdionga, E.; Koonen, T. All-optical multicasting of millimetre-wave signals using optical frequency multiplication technique for in-building networks. In Proceedings of the 2009 35th European Conference on Optical Communication, Vienna, Austria, 20–24 September 2009; pp. 1–2.
15. Kim, H.; Song, H.; Song, J. All-optical Frequency Up-conversion Technique using Four-wave Mixing in Semiconductor Optical Amplifiers for Radio-over-fiber Applications. In Proceedings of the 2007 IEEE/MTT-S International Microwave Symposium, Honolulu, HI, USA, 3–8 June 2007; pp. 67–70.
16. Kim, H.-J.; Song, J.-I. Simultaneous WDM RoF signal generation utilizing an all-optical frequency up converter based on FWM in an SOA. *IEEE Photonics Technol. Lett.* **2011**, *23*, 828–830.
17. Song, H.-J.; Lee, J.S.; Song, J.-I. Signal up-conversion by using a cross-phase-modulation in all-optical SOA-MZI wavelength converter. *IEEE Photonics Technol. Lett.* **2004**, *16*, 593–595. [[CrossRef](#)]
18. Lee, J.S.; Song, H.-J.; Kim, W.B.; Fujise, M.; Kim, Y.-H.; Song, J.-I. All-optical harmonic frequency upconversion of radio over fibre signal using cross-phase modulation in semiconductor optical amplifier. *Electron. Lett.* **2004**, *40*, 1211–1213. [[CrossRef](#)]
19. Song, J.-I.; Song, H.-J. Simultaneous frequency conversion technique utilizing an SOA-MZI for full-duplex WDM radio over fiber applications. *IEICE Trans. Electron.* **2007**, *E90-C*, 351–358. [[CrossRef](#)]
20. Termos, H.; Rampone, T.; Sharaiha, A. All-Optical Radiofrequency Sampling Mixer Based on a Semiconductor Optical Amplifier Mach–Zehnder Interferometer Using a Standard and a Differential Configuration. *J. Light. Technol.* **2016**, *34*, 4688–4695. [[CrossRef](#)]
21. Kastritsis, D.; Rampone, T.; Zoiros, K.E.; Sharaiha, A. Modulation and Switching Architecture Performances for Frequency Up-Conversion of Complex-Modulated Data Signals Based on a SOA-MZI Photonic Sampling Mixer. *J. Light. Technol.* **2020**, *38*, 5375–5385. [[CrossRef](#)]
22. Schreieck, R.P.; Kwakernaak, M.H.; Jackel, H.; Melchior, H. All-optical switching at multi-100-Gb/s data rates with Mach-Zehnder interferometer switches. *IEEE J. Quantum Electron.* **2002**, *38*, 1053–1061. [[CrossRef](#)]
23. Termos, H. Study of up and down Conversion Technique by All Optical Sampling Based on a SOA-MZI. Ph.D. Thesis, Université de Bretagne Occidentale, Brest, France, 2017.
24. Mukherjee, K. Design and analysis of all optical frequency encoded X-OR and X-NOR gate using quantum dot semiconductor optical amplifier-Mach Zehnder Interferometer. *Opt. Laser Technol.* **2021**, *140*, 107043. [[CrossRef](#)]
25. Heydarian, K.; Nosratpour, A.; Razaghi, M. Design and analysis of an all-optical NAND logic gate using a photonic crystal semiconductor optical amplifier based on the Mach–Zehnder interferometer structure. *Photonics Nanostruct.—Fundam. Appl.* **2022**, *49*, 100992. [[CrossRef](#)]
26. Nair, N.; Kaur, S.; Singh, H. All-optical ripple carry adder based on SOA-MZI configuration at 100 Gb/s. *Optik* **2021**, *231*, 166325. [[CrossRef](#)]
27. Capmany, J.; Sales, S.; Pastor, D.; Ortega, B. Optical mixing of microwave signals in a nonlinear semiconductor laser amplifier modulator. *Opt. Express* **2002**, *10*, 183–189. [[CrossRef](#)]
28. Termos, H.; Mansour, A. Frequency Alteration Built on an Electro-Optical Sampling SOA–MZI Using a Differential Modulation Schema. *Optics* **2022**, *3*, 225–233. [[CrossRef](#)]
29. Gomes, N.J.; Monteiro, P.P.; Gameiro, A. *Next Generation Wireless Communications Using Radio Over Fiber*; Wiley: Hoboken, NJ, USA, 2012.
30. Termos, H.; Mansour, A.; Nasser, A. Simultaneous Up and Down Frequency Mixing Based on a Cascaded SOA-MZIs Link. *Appl. Opt.* **2021**, *60*, 8336–8348. [[CrossRef](#)]
31. Termos, H.; Mansour, A. OFDM signal down frequency conversion based on a SOA-MZI sampling mixer using differential modulation and switching architectures. *Optik* **2021**, *245*, 167761. [[CrossRef](#)]
32. Seo, J.-H.; Choi, C.-S.; Kang, Y.-S.; Chung, Y.-D.; Kim, J.; Choi, W.-Y. SOA-EAM frequency up/down-converters for 60-GHz bidirectional radio-on-fiber systems. *IEEE Trans. Microw. Theory Tech.* **2006**, *54*, 959–966.

33. Termos, H.; Mansour, A.; Ebrahim-Zadeh, M. Establishment of an Electro-Optical Mixing Design on a Photonic SOA-MZI Using a Differential Modulation Arrangement. *Sensors* **2023**, *23*, 4380. [[CrossRef](#)]
34. Keysight Technologies. Available online: <https://www.keysight.com/us/en/product/M8194A/120-gsa-s-arbitrary-waveform-generator.html> (accessed on 11 January 2024).
35. VPI Transmission Maker/VPI component Maker, User's Manual, Photonic Modules Reference Manuals. Available online: <http://www.vpiphotonics.com> (accessed on 11 January 2024).
36. Rouvalis, E.; Fice, M.J.; Renaud, C.C.; Seeds, A.J. Millimeter-Wave Optoelectronic Mixers Based on Uni-Traveling Carrier Photodiodes. *IEEE Trans. Microw. Theory Tech.* **2012**, *60*, 686–691. [[CrossRef](#)]
37. Nagatsuma, T.; Ito, H.; Ishibashi, T. High-power RF photodiodes and their applications. *Wiley Laser Photonics Rev.* **2009**, *3*, 123–137. [[CrossRef](#)]
38. Giboney, K.S.; Rodwell, M.J.W.; Bowers, J.E. Traveling-Wave Photodetector Theory. *IEEE Trans. Microw. Theory Tech.* **1997**, *45*, 1310–1319. [[CrossRef](#)]
39. Gazzano, O.; Almeida, M.P.; Nowak, A.K.; Portalupi, S.L.; Lemaître, A.; Sagnes, I.; White, A.G.; Senellart, P. Entangling Quantum-Logic Gate Operated with an Ultrabright Semiconductor Single-Photon Source. *Phys. Rev. Lett.* **2013**, *110*, 250501. [[CrossRef](#)]
40. Biolatti, E.; D'Amico, I.; Zanardi, P.; Rossi, F. Electro-optical properties of semiconductor quantum dots: Application to quantum information processing. *Phys. Rev. B* **2002**, *65*, 075306. [[CrossRef](#)]
41. Akopian, N.; Lindner, N.H.; Poem, E.; Berlatzky, Y.; Avron, J.; Gershoni, D.; Gerardot, B.D.; Petroff, P.M. Entangled photon pairs from semiconductor quantum dots. *Phys. Rev. Lett.* **2006**, *96*, 7–10. [[CrossRef](#)] [[PubMed](#)]
42. Moreau, E.; Robert, I.; Manin, L.; Thierry-Mieg, V.; Gérard, J.M.; Abram, I. Quantum Cascade of Photons in Semiconductor Quantum Dots. *Phys. Rev. Lett.* **2001**, *87*, 183601. [[CrossRef](#)]
43. Krummheuer, B.; Axt, V.M.; Kuhn, T. Theory of pure dephasing and the resulting absorption line shape in semiconductor quantum dots. *Phys. Rev. B* **2002**, *65*, 195313. [[CrossRef](#)]
44. Senellart, P.; Solomon, G.; White, A. High-performance semiconductor quantum-dot single-photon sources. *Nat. Nanotechnol.* **2017**, *12*, 1026–1039. [[CrossRef](#)]
45. Spyropoulou, M.; Pleros, N.; Miliou, A. SOA-MZI-Based Nonlinear Optical Signal Processing: A Frequency Domain Transfer Function for Wavelength Conversion, Clock Recovery, and Packet Envelope Detection. *IEEE J. Quantum Electron.* **2011**, *47*, 40–49. [[CrossRef](#)]
46. Termos, H.; Mansour, A.; Nasser, A. Repetition rate performance for frequency mixing of four simultaneous QPSK signals based on a SOA-MZI photonic sampling mixer. *Opt. Eng.* **2021**, *60*, 116104. [[CrossRef](#)]
47. Schmogrow, R.; Nebendahl, B.; Winter, M.; Josten, A.; Hillerkuss, D.; Koenig, S.; Meyer, J.; Dreschmann, M.; Huebner, M.; Koos, C.; et al. Error vector magnitude as a performance measure for advanced modulation formats. *IEEE Photonic Technol. Lett.* **2012**, *24*, 61–63. [[CrossRef](#)]
48. Shafik, R.A.; Rahman, M.S.; Islam, A.H.M.R. On the extended relationships among EVM, BER and SNR as performance metrics. In Proceedings of the 2006 International Conference on Electrical and Computer Engineering, Dhaka, Bangladesh, 19–21 December 2006; pp. 408–411.
49. Mestre, M.A.; Mardoyan, H.; Caillaud, C.; Rios-Müller, R.; Renaudier, J.; Jennevé, P.; Blache, F. Compact InP-based DFB-EAM enabling PAM-4 112 Gb/s transmission over 2 km. *J. Light. Technol.* **2016**, *34*, 1572–1578. [[CrossRef](#)]
50. 3GPP TS 36.104; Base Station (BS) Radio Transmission and Reception. Version 16; 3GPP: Valbonne, France, 2018.
51. Nguyen, D.-N.; Bohata, J.; Spacil, J.; Dousek, D.; Komanec, M.; Zvanovec, S.; Ghassemlooy, Z.; Ortega, B. M-QAM transmission over hybrid microwave photonic links at the K-band. *Opt. Express* **2019**, *27*, 33745. [[CrossRef](#)] [[PubMed](#)]

Disclaimer/Publisher's Note: The statements, opinions and data contained in all publications are solely those of the individual author(s) and contributor(s) and not of MDPI and/or the editor(s). MDPI and/or the editor(s) disclaim responsibility for any injury to people or property resulting from any ideas, methods, instructions or products referred to in the content.